V.P. KLADKO, O.Y. GUDYMENKO, S.B. KRIVIY, P.M. LITVIN, E.B. KAGANOVICH, I.M. KRISHCHENKO, E.G. MANOILOV

V.E. Lashkaryov Institute of Semiconductor Physics, Nat. Acad. of Sci. of Ukraine
(41, Nauky Ave., Kyiv 03028, Ukraine; e-mail: dept_5@isp.kiev.ua)

PACS 61.43.Gt; 61.46.Df; 61.05.cm; 68.37.-d

REFLECTOMETRY STUDY OF NANOPOROUS FILMS WITH ARRAYS OF GOLD NANOPARTICLES

The influence of conditions occurring at the pulsed laser deposition of films with gold nanoparticles on the film porosity has been studied, by using the X-ray reflectometry. The films of two types were obtained by depositing particles (i) from the direct high-energy flow of erosion-torch particles and (ii) from the backward low-energy one. In both cases, the films were deposited either at the residual air pressure $p = 10^{-2}$ Pa or in the argon atmosphere with the pressures $p_{Ar} = 5$–100 Pa. In case (i), the film porosity was 0.1% at $p = 10^{-2}$ Pa and 1% at $p_{Ar} \leq 5$ Pa. The plasmon properties of those films are associated with the propagation of surface plasmon-polariton waves. As the argon pressure grew further up to 100 Pa, the porosity increased to approximately 30%. In case (ii), the porosity of films deposited at $p_{Ar} = 5$–100 Pa onto substrates located in the target plane equaled 30 to 70% and depended on the distance from the film to the torch axis. All films with the porosity higher than 20% turned out nanocomposite structures with arrays of gold nanoparticles, which enabled us to observe the excitation of local surface plasmons.

Keywords: plasmonics, nanocomposite films, gold nanoparticles, film porosity, pulsed laser deposition method, X-ray reflectometry.

1. Introduction

Films of porous gold (por-Au) are nanocomposites that include gold nanoparticles (Au NPs) and nanopores. The remarkable optical properties of Au NPs are associated with the plasmon absorption of electromagnetic waves. The absorption is responsible for coherent collective oscillations of free electrons that undergo a confinement in nanoparticles. Traditional colloid Au NPs are obtained chemically in the monodisperse form. The dipole absorption peak is also observed in Au NPs imbedded into solid, liquid, and gaseous media. The optical properties of Au NPs depend on the size and shape of nanoparticles, their dielectric environment and spatial organization, the distance between NPs, and the porosity of nanostructures with Au NPs. Those properties determine whether the NPs can be used in optoelectronics, photonics, nanoplasmonics, sensorics, biology, and medicine (as membranes and catalysts), as well as to detect analytes, fabricate substrates for surface enhanced Raman scattering (SERS) of light, enhance the fluorescence of molecules and the photoluminescence of Si and Ge quantum dots, and so forth [1].

A challenging problem is the development of methods to produce films with controlled plasmon properties for sensor nanostructures and SERS substrates. In the latter case, this fact is connected not only with a large internal surface inherent to analytes, but also with the possibility of the formation of "hot spots" in the pores: places with high values of local electromagnetic fields, which are mainly responsible for the enhancement of the Raman scattering by an analyte.

There are known the porous systems, in which the pore walls in aluminum and silicon oxide patterns obtained by the electrochemical etching are covered with a thin layer of noble metals [2]. There are few methods to obtain porous films of gold, which do not demand the application of patterns. In work [3], a technique to form thin mesoporous Au membranes was proposed, which consists in the selective etching of silver from the Ag/Au alloy. Among the vacuum methods aimed at creating the films with arrays of Au(Ag) NPs, the method of pulsed laser deposition (PLD) occupies a special place [4, 5]. Traditionally, the erosion-torch particles from the direct flow are deposited onto a substrate oriented normally to the tar-

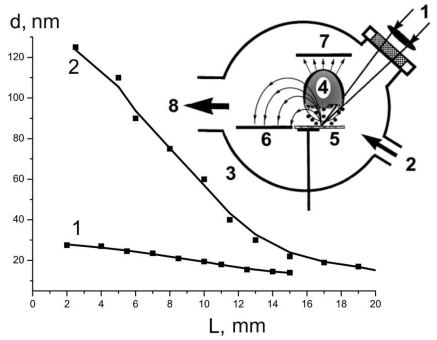

Fig. 1. Dependences $d(L)$ of the thickness of por-Au films (type B) on the distance from the erosion torch axis. The schematic diagram of a vacuum installation for the pulsed laser deposition is shown in the inset: (*1*) laser beam, (*2*) gas inflow, (*3*) vacuum chamber, (*4*) erosion torch, (*5*) target, (*6* and *7*) substrates, and (*8*) vacuum pump

get. In this case, the continuous "nonporous" films are obtained under high-vacuum conditions. In the literature, we did not find the results of researches concerning the porosity of films with arrays of Au(Ag) NPs produced by the PLD method even at substantial gas pressures in the chamber.

In our previous works [6–9], we fabricated porous films (por-Si(Ge), por-Al_2O_2, por-Au(Ag)) using the PLD method and depositing erosion-torch particles from the backward flow onto a substrate located in the target plane. The structural and optical properties of those films were partially analyzed, and some possibilities of their application to optoelectronics and sensorics, as well as SERS substrates, were demonstrated. However, not enough information was obtained concerning the film porosity, its dependence on the formation conditions, and the influence of the porosity of a film on its optical properties. This circumstance partially follows from the fact that the methods applied to characterize the porosity of thin films lag behind the technologies of film formation.

The methods of registration of the porosity in nanostructures by monitoring the gas adsorption, density (gravimetric researches), and optical properties in the framework of effective medium models are known. Among them, the method of X-ray reflectometry, which is based on the effect of total external reflection (TER) of X-rays from examined specimens, has substantial advantages. The value of critical angle $\theta_{\rm cr}$ determined with the use of this method includes information concerning the film density, which can be used to find the film porosity [10–12]. The literature contains data on the measurements of film densities for the determination of the porosity in por-Si layers [11, 12], for the researches of the laser-assisted evaporation of SiO_2 films from the silicon surface [10], and so on. We know nothing about the application of the X-ray reflectometry method to the investigation of the porosity of gold films. This work aims at studying the influence of the film formation conditions at the pulsed laser deposition of gold films on their porosity using the X-ray reflectometry method and analyzing the relation between the porosity and the plasmon properties of gold films.

2. Experimental Technique

Films with an array of Au NPs were produced, by using the method of pulsed laser deposition (see the inset in Fig. 1) of erosion-torch (*4*) particles from the direct and backward flows in vacuum chamber (*3*) with a residual pressure of 10^{-2} Pa or the argon pressure (*2*) $p_{\rm Ar} = 5 \div 100$ Pa onto substrates (*7* and *6*) located at a some distance from the target and in its plane, respectively. The beam of YAG:Nd^{3+} laser (*1*) with a wavelength of 1.06 μm, a pulse energy of 0.2 J, a pulse duration of 10 ns, and a pulse recurrence rate of 25 Hz was used to scan target (*5*) composed of small gold pieces. The energy density in the pulse fell within the interval $j = 5 \div 20$ J/cm^2. The pulse number N was varied from 3×10^4 to 6×10^4. While depositing films from the backward flow of erosion-torch particles, the nanostructures formed on the substrate near the torch axis had larger thicknesses and larger sizes of Au NPs than those located at some distance from the torch axis. Hence, besides three deposition parameters p, j, and N, there also exists the fourth one, L, the distance from the film section to the torch axis.

Reflectometry researches were carried out on a PANalitical's high-resolution X-ray diffractometer X-Pert PRO MDR using the characteristic $Cu_{K\alpha 1}$ radiation. The X-ray monochromatization was done with the help of a four-crystal Ge(220) monochromator. The reflectometry curves were fitted making use of the software program X'Pert Reflectivity, which allowed us to obtain information concerning the film density, roughness, and thickness (provided the presence of thickness oscillations). The determined film density $\rho_{\rm exp}$ was used to find the film porosity by the formula $\Pi = (1 - \rho_{\rm exp}/\rho_m) \times 100\%$, where ρ_m is the density of a massive substance.

While studying the films by the method of surface plasmon-polariton resonance in the Kretschmann geometry, a Plasmon-6 spectrometer developed at V.E. Lashkaryov Institute of Semiconductor Physics of the National Academy of Sciences of Ukraine was used. The angular dependences of the frustrated total internal reflection were approximated in the framework of the optical model on the basis of Fresnel equations. The effective values of the refractive index n_{eff}, extinction coefficient κ_{eff}, and film thickness d were calculated with the help of the software program WinSpall 3.02 [13].

To analyze the results obtained, they were compared with the research data on the surface morphology and the thickness of films measured on an atomic-force microscope NanoScope IIIa (Digital Instruments) in a mode of periodic contact and using silicon probes with a tip of 10 nm in nominal radius. For por-Au films, the vertical and horizontal sizes of Au NPs and dips, which the film surface consisted of, were evaluated. For the determination of a film thickness, the height of substrate–film steps formed by the method of explosive lithography was measured.

The transmission spectra of films were measured with the help of a SF-26 spectrophotometer in a wavelength interval of 360–1000 nm.

3. Results and Their Discussion

In Fig. 1, the results of AFM measurements for the dependences of the film thickness d on the distance L from the substrate point to the torch axis are depicted for the films deposited from the backward flow of erosion-torch particles. The films obtained at the deposition parameters $j = 5$ J/cm^2 and $N = 3\times10^4$ are different for the argon pressures $p_{\text{Ar}} = 100$ (curve *2*) and 13.5 Pa (curve *1*). Figure 1 demonstrates that the thickness profile is almost wedge-like, and the film thickness decreases, as the distance from the torch axis grows. The film obtained at $p_{\text{Ar}} = 100$ Pa (curve *2*) reveals a steeper reduction of the thickness at $L < 15$ mm and a more sloping dependence at large distances from the torch axis (from 15 to 25 mm). The dependence $d(L)$ for the film deposited at $p_{\text{Ar}} = 13.5$ Pa is sloping everywhere. From Fig. 1, it is evident that the film thickness considerably grows (up to $d = 120$ nm) at the points located near the torch axis if the argon pressure in the chamber increases to $p_{\text{Ar}} = 100$ Pa.

It was shown that, similarly to the argon pressure growth, the increase in the number of pulses irradiating the target to $N = 6 \times 10^4$ and the energy density in the pulse to $j = 20$ J/cm^2 also results in the film thickness growth. The thicknesses were almost identical at the following sets of parameters: (i) $j = 5$ J/cm^2, $p = 20$ Pa, and $N = 3 \times 10^4$;(ii) $j = 20$ J/cm^2, $p = 13.5$ Pa, and $N = 3 \times 10^4$; and (iii) $j = 5$ J/cm^2, $p = 13.5$ Pa, and $N = 6 \times 10^4$. The film thickness itself varied from a few nanometers to about 100 nm.

Figure 2, *a* exhibits the AFM images of the por-Au film deposited at $p = 100$ Pa, $j = 5$ J/cm^2, and $N = 30\,000$ (curve *2* in Fig. 1), which were obtained for areas around two points located at distances of 5 and 15 mm from the torch axis. The results of the cross-section analysis are shown in Fig. 2, *b*, and the histograms of the Au NP and dip size distributions over those two areas of the film in Fig. 2, *c*. The analysis of the film surface morphology testifies to the presence of an ensemble of Au NPs, as well as dips between them with comparable dimensions and concentration. The dimensions of Au NPs and pores achieve tens nanometers at the points nearest to the torch axis and several nanometers at the most distant ones. The film thickness is of the same order of magnitude as the sizes of Au NPs and dips.

In Fig. 3, *a*, the curves of the X-ray specular reflection are shown for films obtained by depositing the erosion-torch particles from the direct flow (films of the first type, films D) (curves *2* to *5*), and for a film thermally deposited in vacuum (curve *1*). The same curves, but for films obtained by depositing the erosion-torch particles from the backward flow (films of the second type, films B), are depicted in Fig. 3, *b*. The corresponding conditions of the film formation and the calculated values of film parameters are quoted in Table.

The obtained results of reflectometry researches concerning the film porosity and its dependence on the film formation conditions can be summarized as follows. The por-Au films deposited from the direct flow of erosion-torch particles are characterized by the porosity within an interval of 0.1–30%, and those deposited from the backward flow within an interval of 30–70% (see Table). Accordingly, films D are characterized by the highest density close to the density of massive polycrystalline gold, whereas films B by the lowest one. It should be noted that the density of

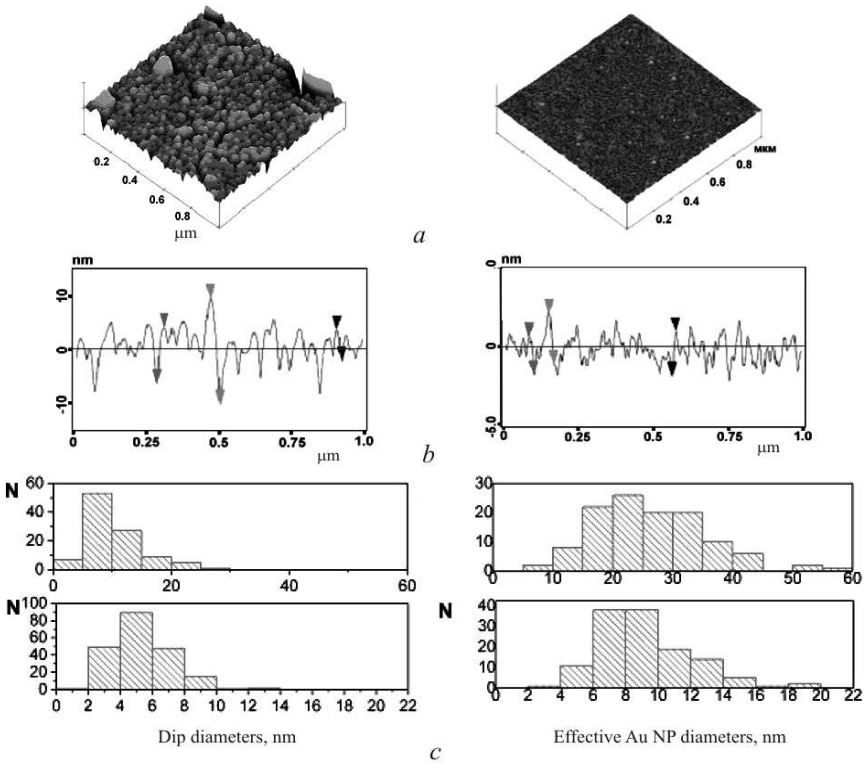

Fig. 2. (*a*) AFM images of fragments on the por-Au film surface ($j = 5$ J/cm^2, $N = 3{\times}10^4$, $p_{\rm Ar} = 100$ Pa). (*b*) The corresponding cross-sectional analysis. Left panel corresponds to the near film section, and right panel to the far one. (*c*) Histograms for the sizes of dips and Au NPs. Upper panels correspond to the near film section, and lower panels to the far one

films D deposited at $p = 10^{-2}$ Pa (D33) is higher than the density of the films obtained by thermal sputtering (AuT). Their porosity is $\Pi \approx 0.1\%$ (curve *2* in Fig. 3, *a*). At $p_{\rm Ar} = 5$ Pa, the film porosity (D49) does not exceed a few percent (curve *3* in Fig. 3, *a*); but already starting from $p_{\rm Ar} = 10 \div 13.5$ Pa (D46–D34), it grows to 20–30% (curves *4* and *5* in Fig. 3, *a*). Hence, the film porosity substantially depends on the argon pressure at $p_{\rm Ar} \geq 10$ Pa. At the same time, the variations of the energy density in a pulse within an interval of 5–20 J/cm^2 and the pulse number within an interval of 3×10^4 to 6×10^4 do not result in substantial porosity changes. The dependence of the film porosity on the pressure in the chamber is associated with the fact that, if the pressure increases, the energies of atoms and clusters are scattered by gas atoms, so that the films are formed from nanoparticles with lower energies. The number of atoms in Au NPs drastically grows, and their sizes reach up to 10 nm (see also work [5]). The deposition of such Au NPs results in the emergence of porous structures, whereas, at a residual pressure of 10^{-2} Pa, the films that are formed from high-energy Au NPs with small dimensions are the most solid and "nonporous".

The simulation of theoretical reflectometry curves and their further fitting demonstrated that, at low gas pressures in the chamber, the film roughness is low (RMS < 1 nm), and the film thickness $d \approx 50$ nm. At the argon pressures $p_{\rm Ar} \geq 10$ Pa, the film roughness increases to 1–2.6 nm, and the film thickness decreases to $d \approx 10$ nm. Such a character of the dependences of film parameters on the gas pressure correlates with the reduction of the nanoparticle energy and the growth of nanoparticle sizes.

A characteristic feature in the formation of films of the second type (films B) is the separation of Au NPs and pores on the substrate according to their sizes (see Fig. 2). The obtained values of film porosity should be considered as effective averaged ones, which is associated with the gradients of the film thickness and NP and pore dimensions. At the large values of thickness gradient (see curve *2* in Fig. 1),

the porosities of film sections near to (*1*) and far from (*2*) the torch axis are different: 64.5 and 36.4%, respectively (see film B5 in Table, and curves 1 and 5 in Fig. 3, *b*). At the same time, if the thickness gradient is small (see curve *1* in Fig. 1), the film porosities are almost identical: 27.9 and 34.2%, respectively (see film B7 in Table, and curves *4* and *6* in Fig. 3, *b*).

At the residual pressure in the vacuum chamber $p = 10^{-2}$ Pa, the film thickness is too small even if $j = 20\,\mathrm{J/cm^2}$ and $N = 60000$. At the low argon pressure $p_{\mathrm{Ar}} = 5$ Pa, thin films (≈10 nm) are formed (film B9, curve *2* in Fig. 3, *b*). In this case, the film thickness and the size of Au NPs and pores are comparable. Therefore, the low density of this film ($\rho = 6.71\,\mathrm{g/cm^3}$) and, respectively, its high porosity ($\Pi = 65.2\%$) can result from a considerable number of pores with small dimensions. At high argon pressures $p_{\mathrm{Ar}} = 50$ and 100 Pa (films B19, B5, and B38), thick films with large dimensions of Au NPs and pores are formed, and their high porosity ($\Pi = 60 \div 70\%$) is caused by a small number of pores with substantial sizes.

At the argon pressure $p_{\mathrm{Ar}} = 13.5$ Pa, the films (films B6–B8) are characterized by the porosity $\Pi = 30 \div 54\%$ (see also curve *3* in Fig. 3, *b* for film B6). At the constant parameters $p_{\mathrm{Ar}} = 13.5$ Pa and $N = 3 \times 10^4$, the increase of the energy density in a pulse from $j = 5$ to 20 J/cm^2 (cf. films B6(1) and B7(1)) gives rise to the growth in the number of gold atoms in the torch owing to a change of the ablation mode. Therefore, the thickness of a deposited film changes from about 11 to about 25 nm, its density also increases from 8.5 to 13.92 g/cm^3, and, accordingly, the porosity decreases from 54.7 to 27.9%. At $p_{\mathrm{Ar}} = 13.5$ Pa and $j = 20$ J/cm^2, the growth of the pulse number from 3×10^4 (film B6(2)) to 6×10^4 (film B8(2)) gives rise to the increase of the film thickness by more than a factor of 2 (from about 13 to about 30 nm), which is responsible for the density growth from $\rho = 8.95$ to 12.25 g/cm^3. Accordingly, the porosity decreases from 53.6 to 36.5%.

Formation conditions for films deposited from the direct (D) and backward (B) flows of erosion-torch particles and the resulting film density ρ and porosity Π

Films	Formation conditions			Film parameters	
	p, Pa	j, J/cm^2	N, 10^3	ρ, g/cm^2	Π,%
TAu	0.01	–	–	18.79	2.6
D33	0.01	20	60	19.28	0.1
D49	5	20	60	19.1	1.0
D46	13.5	20	60	15	22.3
D45	13.5	5	30	14.3	25.9
D18	13.5	20	30	14.19	26.5
D34	50	20	30	13	32.6
B9(2)	5	20	30	6.71	65.2
B7(1)	13.5	20	30	13.92	27.9
B7(2)	13.5	20	30	12.7	34.2
B6(1)	13.5	5	30	8.75	54.7
B8(2)	13.5	20	60	12.25	36.5
B19(2)	50	20	30	7	63.7
B5(1)	100	5	30	6.86	64.5
B38(1)	100	20	30	7	63.7
B38(2)	100	20	30	5.8	69.9

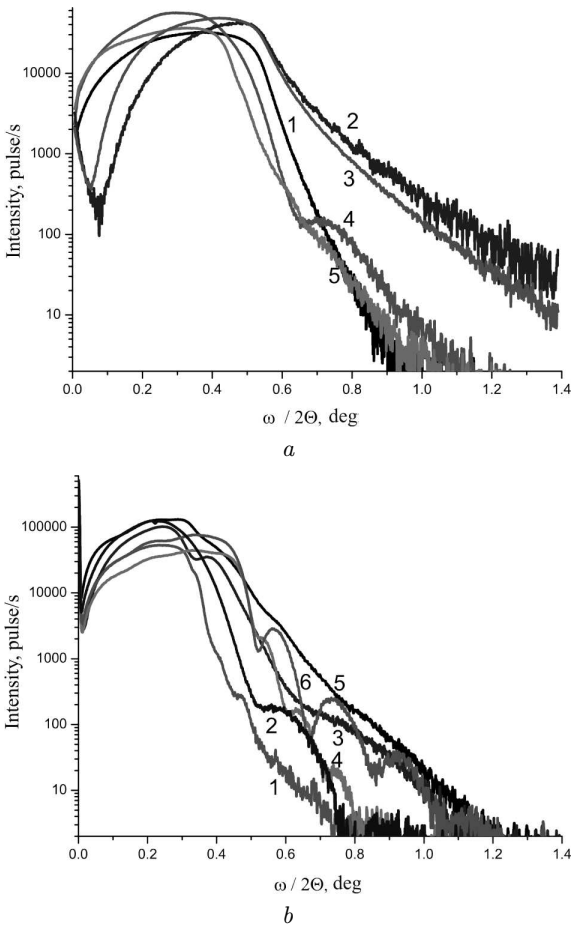

Fig. 3. X-ray specular reflection curves for films: (*a*) AuT (*1*), D33 (*2*), D49 (*3*), D18 (*4*), and D34 (*5*); (*b*) B5(1) (*1*), B9(2) (*2*), B6(1) (*3*), B7(1) (*4*), B5(3) (*5*), and B7(2) (*6*)

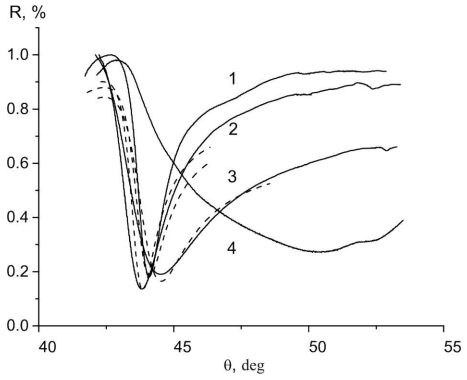

Fig. 4. Angular dependences of the frustrated total internal reflection coefficient R_{FTIR} for films obtained by the thermal sputtering (*1*), films D deposited at a residual pressure of 10^{-2} Pa (*2*) and argon pressures of 5 Pa (*3*) and 10 Pa (*4*). Solid curves exhibit experimental data, and dashed ones correspond to theoretical results

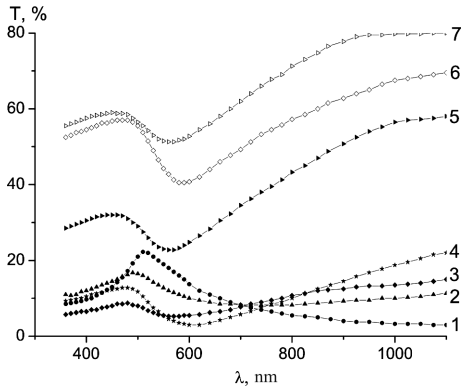

Fig. 5. Transmission spectra of films D (curves *1*, *2*, and *4*) and B (curves *3* and *5–7*). Parameter values: $p = 10^{-2}$ (*1*), 10 (*2*), 13.5 (*5* and *7*), 50 (4), and 100 Pa (*3* and *6*); $j = 5$ (*3* and *5–7*) and 20 J/cm^2 (*1*, *2*, and *4*); $N = 30000$ (*3–7*), 45000 (*1*), and 60000 (*2*); $L = 5$ (*3–5*) and 15 mm (*6* and *7*)

For the indicated technological parameters, the average thicknesses of the films belonging to the second type (films B) fall within the interval of 10–40 nm, and the surface roughness equals RMS ≈ 2 nm. The determined values of film thickness are close to those obtained, by using the AFM method.

In Fig. 4, the angular dependences of the intensity of the frustrated total internal reflection (FTIR) $R_{\mathrm{FTIR}}(\theta)$ for films D (curves *2* to *4*) and a thermally sputtered gold film (curve *1*) are depicted. Curve *2* demonstrates that the film deposited at the residual pressure $p = 10^{-2}$ Pa is in the regime of the surface plasmon-polariton resonance if it is irradiated with *p*-polarized light with $\lambda = 640$ nm. The $R_{\mathrm{FTIR}}(\theta)$ curve for this film almost coincides with its counterpart for the thermally sputtered film. However, the minimum $\theta_{\min}$ for film D is shifted toward smaller values. This fact testifies to a somewhat smaller refractive index of the film. Provided that the thicknesses of the films are close, this means the lower porosity of film D. It should be noted that this result coincides with that obtained using the X-ray reflectometry method. From curve *3* in Fig. 4, one can see that, for film D obtained at the argon pressure $p_{\mathrm{Ar}} = 5$ Pa, the position $\theta_{\min}$ of the curve $R_{\mathrm{FTIR}}(\theta)$ is shifted toward larger angles in comparison with the previous film D (curve *2*). This means that, since the thicknesses of those films are close, the refractive index and the film porosity grow. This result also coincides with that obtained, by using the X-ray reflectometry method.

Calculations carried out in the framework of the optical model gave us the following parameter values: for the film AuT, $n_{\mathrm{eff}} = 0.371$, $k_{\mathrm{eff}} = 3.57$, and $d = 51.62$ nm; for the film D33, $n_{\mathrm{eff}} = 0.34$, $k_{\mathrm{eff}} = 3.76$, and $d = 46.13$; and for the film D49, $n_{\mathrm{eff}} = 0.48$, $k_{\mathrm{eff}} = 3.37$, and $d = 49.69$ nm (see Table and Fig. 4). It should be noticed that the film AuT was obtained by the thermal sputtering in vacuum without creating any conditions to improve its structure. The determined n_{eff}-values turned out expectedly smaller for less porous films (film D33) and larger for more porous ones (film D49), because $n_{\mathrm{air}} = 1$ and $n_{\mathrm{Au}} \approx 0.33$. The corresponding determined values of film thicknesses, $d \approx 50$ nm, coincide with those obtained using the X-ray reflectometry method.

In Fig. 4, curve *4* corresponds to film D deposited at $p_{\mathrm{Ar}} = 10$ Pa. One can see that the growth of the argon pressure gives rise to a violation of the conditions required for the surface plasmon-polariton resonance regime. Those conditions are not satisfied for all films of type B.

In Fig. 5, the transmission spectra $T(\lambda)$ for the films obtained are depicted. This figure illustrates the difference between the optical properties of films in two groups. For film D deposited from the direct flow of erosion-torch particles at $p = 10^{-2}$ Pa (curve *1* in Fig. 5), light is strongly absorbed in the near IR and visible spectral ranges as a result of the absorption by free carriers. For all films B (curves *3* and *5* to *7* in Fig. 5), light with the wavelengths more than about 650 nm is not absorbed. Those films reveal pronounced absorption peaks in the interval of

550–600 nm, which are related to the excitation of local surface plasmons (LSPs) on the Au NPs. For both groups of films, the characters of spectra in the interval of 350–450 nm are similar, being governed by *d-sp* interband transitions. The influence of every of p, j, N, and L parameters on the character of the dependence $T(\lambda)$ for films B, as well as the fact that the optical properties of films with LSPs are determined by the set of all those parameters, is illustrated by curves *3* and *5* to *7* in Fig. 5.

4. Conclusions

X-ray reflectometry is applied for the first time to determine the influence of the formation conditions at the pulsed laser deposition of nanocomposite films with an array of plasmonic gold nanoparticles on the film porosity. The relationships between the porosity and the plasmon properties of the examined nanostructure are found. It is shown that the deposition of gold films from the direct flow of high-energy erosion-torch nanoparticles at the residual pressure lower than 10^{-2} Pa makes it possible to obtain films with a low porosity of 0.1%. Such films can be recommended for the application in optical sensors operating on the basis of the surface plasmon-polariton (PP) wave excitation. As the argon pressure in the chamber increases to 50–100 Pa, the film porosity grows up to 30%. At $p = 10$ Pa, the films do not demonstrate the PP resonance, and the conditions for the excitation of a local surface plasmon (LSP) resonance are not realized as well. Those conditions are only improved a little for films with a porosity of 25–30%.

The pulsed laser deposition from the backward flow of erosion-torch particles allows one to obtain the nanocomposite porous (with a porosity of 30–70%) films with an ensemble of plasmonic Au NPs. The film thickness (less than 50 nm) is comparable with the sizes of Au NPs and pores (from several nanometers to 10–20 nm). The set of technological parameters – the argon pressure (10^{-2}–100 Pa), the number of pulses (3×10^4–6×10^4), the energy density in the pulse (5–20 J/cm^2), and the distance from the film section to the torch axis (5–20 mm) – determine the LSP absorption spectrum in the wavelength interval of 550–800 nm. The plasmon characteristics of those films are favorable for them to be used in fabricating SERS substrates for the surface enhancement of the Raman scattering by the analyte.

1. E. Le Ru and P. Etchegoin, *Principles of Surface Enhanced Raman Spectroscopy and Related Plasmonic Effects* (Elsevier, Amsterdam, 2009).
2. S.N. Terekhov, P. Mojzes, S.M. Kachan, N.J. Mukhurov *et al.*, J. Raman Spectrosc. **42**, 12 (2011).
3. F. Yu, S. Ahl, A.-M. Caminade *et al.*, Anal. Chem. **78**, 7346 (2006).
4. A.V. Kabashin and M. Meunier, in *Recent Advances in Laser Processing of Materials,* edited by J. Perriere, E. Millon, and E. Fogarassy (Elsevier, Amsterdam, 2006), Chap. 1.
5. N.R. Agarwal, F. Neri, S. Trusso *et al.*, Appl. Surf. Sci. **258**, 9148 (2012).
6. P.M. Litvin, O.S. Litvin, I.V. Prokopenko *et al.*, Nanosyst. Nanomater. Nanotekhnol. **1**, 601 (2004).
7. E.B. Kaganovich, E.G. Manoilov, and E.V. Begun, Fiz. Tekh. Poluprovodn. **41**, 177 (2007).
8. Yu.V. Ushenin, R.V. Khristosenko, A.V.Samoilov *et al.*, Optoelektron. Poluprovodn. Tekhn. **47**, 40 (2012).
9. E.B. Kaganovich, S.A. Kravchenko, L.S. Maksimenko*et al.*, Opt. Spektrosk. **110**, 552 (2011).
10. A.P. Petrakov, Zh. Tekhn. Fiz. **73**, 129 (2003).
11. L.A. Balagurov, V.F. Pavlov, E.A. Petrov, and G.P. Boronina, Fiz. Tekh. Poluprovodn. **31**, 957 (1997).
12. V.V. Ratnikov, Fiz. Tverd. Tela **39**, 956 (1997).
13. http://www.mpip-mainz.mpg.de/∼johanns/ak_knoll_Software.htm

Received 26.05.14.
Translated from Ukrainian by O.I. Voitenko

В.П. Кладько, О.Й. Гудименко, С.Б. Кривий, П.М. Литвин, Е.Б. Каганович, І.М. Кріщенко, Е.Г. Манойлов

РЕФЛЕКТОМЕТРИЧНІ ДОСЛІДЖЕННЯ НАНОПОРИСТИХ ПЛІВОК З МАСИВОМ НАНОЧАСТИНОК ЗОЛОТА

Р е з ю м е

Вивчено вплив умов формування імпульсним лазерним осадженням плівок з наночастинками золота на їх пористість із застосуванням рентгенівської рефлектометрії. Одержано плівки двох типів: з прямого високоенергетичного та зворотного низькоенергетичного потоків частинок ерозійного факела при залишковому тиску $p = 10^{-2}$ Па і тиску аргону $p_{\rm Ar} = 5$–100 Па. Встановлено, що пористість плівок першого типу, одержаних при $p = 10^{-2}$ та $p_{\rm Ar} \leqslant 5$ Па, становить 0,1 і 1%. Для цих плівок плазмонні властивості пов'язані з поширенням поверхневих плазмон-поляритонних хвиль. З подальшим підвищенням тиску аргону до 100 Па пористість зростає до ≈30%. Показано, що для плівок другого типу, осаджених при $p_{\rm Ar} = 5$–100 Па на підкладку, яка розташована в площині мішені, пористість становить 30–70% та залежить від положення ділянки плівки відносно осі факела. Всі плівки з пористістю більшою за 20% є нанокомпозитними структурами з масивами наночастинок золота. На них спостерігається збудження локальних поверхневих плазмонів.